Forcing Mechanisms Controlling Surface and Subsurface Temperature Anomalies along Line-P, Northeast Pacific Ocean

Alexandre Laîné[1], William W. Hsieh[1] and Howard J. Freeland[2]

[1] *Department of Earth and Ocean Sciences, University of British Columbia, Vancouver, BC, V6T 1Z4*

[2] *DFO Science, Pacific Region, Institute of Ocean Sciences, Sidney, BC, V8L 5R4*

Submitted to Atmosphere-Ocean

14th September, 2004

Corresponding author: William Hsieh, Department of Earth and Ocean Sciences, 6339 Stores Road, Vancouver, BC V6T 1Z4

e-mail: whsieh@eos.ubc.ca

tel.: 604-822-2821, fax: 604-822-6088

Abstract

The influence of different mechanisms on surface and subsurface temperature anomalies is considered along Line-P, an oceanographic line extending from Vancouver Island into the Gulf of Alaska, sampled for almost half a century. The role of a given mechanism is determined by applying canonical correlation analysis (CCA) between the anomalies of a parameter representing the mechanism and the Line-P temperature anomalies. For each mechanism, it is determined if its direct influence can be detected, and if so, the domain of Line-P over which it acts.

Two areas along Line-P, characterized by different forcing mechanisms, have been identified: (1) offshore, west of 130^oW, the main mechanisms influencing Line-P temperature anomalies are the Ekman transport due to wind stress anomalies (with the zonal wind stress component somewhat more important than the meridional component) and wind mixing anomalies, (2) from the coast to 180 km offshore, coastal upwelling/downwelling anomalies and sea surface height anomalies along the coast of North America, resulting in coastal current anomalies and/or northward propagation of coastal waves, are important in determining Line-P temperature anomalies.

1 Introduction

The region considered in the present study is located in the northeast Pacific (NEP), and is studied using data from Line-P, an oceanographic survey line extending from 35 km offshore Vancouver Island to Ocean Station Papa (OSP), [50^oN; 145^oW], in the Gulf of Alaska (Fig. 1).

The climatological conditions in the region surrounding Line-P is also shown in Fig. 1. A broad current, called the North Pacific Current or the West Wind Drift, flows eastward and constitutes the northern limb of the clockwise sub-tropical gyre and the southern limb of the counterclockwise Alaska gyre. When it approaches the coast of Vancouver Island, it splits between a northward flow entering the Alaskan gyre, to constitute the Alaska Current (called the Alaskan Stream in the western part of the gulf), and a southward current entering the California Current System. At the order of tens of kilometres from the shore, coastal currents can also be found, driven by fresh water inputs and by wind through upwelling (Royer, 1981).

In summer, the North Pacific High dominates the NEP and implies upwelling-favourable winds all along the coast of North America, coinciding with the strongest southward California Current. In winter, the extension and deepening of the Aleutian Low in the Gulf of Alaska leads to downwelling-favourable (poleward) winds along the West coast of America northward of approximately 37°N, consistent with the strongest Alaska Current and the weakest or even reversed California Current (Strub and James, 2002a). Winter is also the stormy season, during which the wind speed reaches its highest values in the NEP.

This general situation is a simple climatological sketch of the circulation in the NEP, and from one year to another, the physical state in the region can be significantly different. Upper-ocean temperature anomalies (departing from the mean seasonal cycle) is one par-

ticularly important parameter for considering the physical and ecological state in the ocean and also inland. For instance, the sea surface temperature (SST) variability in the Gulf of Alaska has been related to the return of the Fraser River Sockeye Salmon (McKinnell et al., 1999), snow and streamflow in British Columbia (Hsieh and Tang, 2001; Hsieh et al., 2003), Canadian prairie wheat yield (Hsieh et al., 1999) and also first bloom dates in Alberta (Beaubien and Freeland, 2000).

Interannual variability is primarily related to El Niño-Southern Oscillation (ENSO) events, which modify oceanic conditions along all of the eastern Pacific margin. The influence of the tropical Pacific occurs through different dynamical processes. The warm surface water accumulating in the eastern equatorial Pacific during El Niño events imply a deepening of the thermocline and an elevation of the sea surface at the coast, which propagate as coastally trapped waves from the equator up to the coast of Alaska (Enfield and Allen, 1980; Huyer and Smith, 1985). This signal can modify the temperature field along Line-P close to the coast due to a displacement of the thermocline (resulting in temperature anomalies around its usual depth) or due to current anomalies (and a subsequent displacement of the mean alongshore temperature gradient), through geostrophic adjustment resulting from changes in sea surface heights at the coast.

Stronger alongshore winds are also usually associated with strong El Niños (ENs) (weaker during strong La Niñas (LNs)), resulting in stronger (weaker) coastal downwelling in winter, thus changing the temperature, salinity and nutrient conditions at the coast (Simpson, 1984). The influence of anomalous coastal upwelling or downwelling on the temperature field comes from an increased rate of cold deep water being upwelled or warm upper-layer water being downwelled, and also from coastal current anomalies resulting from sea surface height changes at the coast. The alongshore wind anomalies may be part of large-scale atmospheric

pressure systems arising from the atmospheric response to equatorial SST anomalies during EN or LN events (Schwing et al., 2002). The relative importance of oceanic and atmospheric mechanisms during ENSO events in explaining the coastal anomalies depends on the region considered. The influence of the oceanic connection is stronger from the equator to the Gulf of California, whereas local and basin-scale winds usually have a predominant effect farther north up to the Alaskan Peninsula (Strub and James, 2002b; Qiu, 2002; Enfield and Allen, 1980).

Variability of oceanic conditions in the northeast Pacific also occurs over interdecadal time scales. During the twentieth century, radical shifts on large scales in the North Pacific (around 1947 and 1977) have first been noticed in marine biology (Kawasaki, 1983; Lluch-Belda et al., 1989). Later, Mantua et al. (1997) introduced an index, the Pacific Decadal Oscillation (PDO) (defined as the leading principal component of monthly SST over the North Pacific since 1900), which is correlated to many North Pacific climatic and biological time series (Chavez et al., 2003).

Although most of the large scale variability can be related to either ENSO or the PDO, some extreme conditions can occur in the NEP that appear to be independent of either mode of variability. For example, extreme conditions were observed in summer 2002 over more than 1500 km along the California Current. Strong negative temperature anomalies, never observed before despite decades of records, were found in July 2002 between 30 and 150 m depth off Oregon and Vancouver Island (Freeland et al., 2003). Southward advection of temperature anomalies in the California Current during spring and summer 2002 (Barth, 2003; Kosro, 2003), as well as zonal advection anomalies in the North Pacific Current (Strub and James, 2003), are at least part of the explanation. The current anomalies themselves seemed to be caused by large-scale atmosphere-ocean processes (Murphree et al., 2003).

Nevertheless, other mechanisms might also have played a role leading to these extreme conditions.

Other processes which might influence upper ocean temperature anomalies include the wind mixing, Ekman pumping, Sverdrup balance, sensible and latent heat transfers, and radiative forcing. Positive wind speed anomalies result in a stronger turbulent mixing between relatively warm surface water and colder deep water, leading to upper-layer ocean temperature anomalies. Basin-scale wind changes can also result in wind stress curl anomalies at the surface, which would imply upwelling anomalies through Ekman pumping, or meridional current anomalies following the Sverdrup balance. Anomalous atmospheric pressure systems may also disturb the usual heat and humidity content of the air advected over specific regions of the NEP, thus changing the sensible and latent heat transfers and eventually the radiative balance from different cloud cover and cloud composition.

The aim of this study is to understand the general behavior of Line-P temperature anomalies by determining the dominant forcing mechanisms influencing them. This knowledge is fundamental to understand NEP upper-ocean temperature anomalies, which have a wide range of physical and ecological impacts inland or in the ocean. It could also be a first step to understand the temperature anomalies associated with ENSO events and the PDO index through their connections to specific forcing mechanisms.

This paper starts with a presentation of the data and the specific technique used to relate given forcing anomalies to temperature anomalies along Line-P (Section 2). We then present the results for mechanisms found to be dominant *a posteriori*. They include the displacement of the mean temperature gradient due to Ekman transport anomalies in the zonal and meridional directions (Sec. 3.1), wind mixing process (Sec. 3.2), coastal upwelling and downwelling (Sec. 3.3), coastal wave propagation and coastal current anomalies along

the west coast of the United States (Sec. 3.4). The results for the other forcing mechanisms whose anomalies could not be correlated to Line-P temperature anomalies using our technique, thus considered to have a minor influence, are briefly discussed in Section 3.5 (Ekman pumping, Sverdrup balance, sensible and latent heat fluxes, solar and long-wave radiation, the advection of temperature anomalies along the North Pacific Current and Alaska Current anomalies), along with a discussion on the limitations of the technique used. Finally, Section 4 provides the conclusions of the present work.

2 Data and Method

2.1 Data

The original data consist of hydrographic casts performed along Line-P from May 1956 to September 2002, which include measurements of temperature, salinity and pressure. The samples were first restricted to the farthest station P13, also called Ocean Station Papa (OSP), and were gradually performed at different locations along the line, until the 13 stations were definitively established in August 1964. The sampling along Line-P was frequent until June 1981 (approximately every 6 weeks), and was later carried out at a rate of 2 to 6 times per year. A more complete history of Line-P sampling is presented in Whitney and Freeland (1999).

Since the depth range and the vertical sampling intervals are different from one cast to another, we interpolated temperature values to every 5 m to get a standard format. We worked with the data from the surface to 500 m depth. To get monthly data, we averaged all the values available in a given month for every depth increment. In most cases, the resulting monthly datum was only derived from a few casts, and should be carefully considered,

especially at the surface where conditions may vary daily. It is a less important issue at greater depths where temperature is expected to vary on longer time scales. Nevertheless, larger depth intervals at greater depths lead to inacurracies in the interpolation.

Zonal wind, meridional wind and wind speed data consist of monthly means obtained from the Climate Diagnostics Center (CDC) Derived National Centers for Environmental Prediction (NCEP) Reanalysis Products. Temporal coverage spans the Line-P sampling period. Spatial coverage is global with a 2.5-degree resolution both in latitude and longitude. NCEP Reanalysis data are provided by the NOAA-CIRES Climate Diagnostics Center, Boulder, Colorado, USA, from their web site at http://www.cdc.noaa.gov.

Climatological ocean temperature values came from the National Oceanographic Data Center (NODC) (Levitus) World Ocean Atlas 1998 (http://www.cdc.noaa.gov/cdc/data.nodc.woa98.html), containing global data with a resolution of 1 degree in latitude and longitude, for various depths.

Monthly values for the zonal and meridional wind stresses are directly obtained by multiplying the monthly means of the wind speed by the wind component in the given direction. The wind stress is defined as $\overrightarrow{\tau} = \rho_A c_D \, \| \overrightarrow{u} \| \, \overrightarrow{u}$, where $\overrightarrow{u}$ is the wind vector, ρ_A the air density and c_D the drag coefficient. In this study, we only use time series of the wind stress anomalies for correlation purposes. Multiplying a time series by a constant does not change the results of a correlation, so the fact that we do not consider the density of air and the drag coefficient is equivalent to assuming them to be constant. It is an approximation since the density of air may vary and since the drag coefficient is a function of the wind speed. Another approximation results from reconstructing wind stress monthly means from the monthly values of the wind speed and of the wind component, instead of using daily winds for example. This may weaken the difference between the monthly values of the

wind and the wind stress components. Indeed, using the wind components instead of those reconstructed wind stress components in sections 3.1 and 3.3 gives similar results.

2.2 Method

2.2.1 Method description

We want to consider the direct effect of the anomalies of a given forcing field on the Line-P temperature field. For that, we take advantage of the unique length of Line-P records (one of the longest in the history of oceanographic lines) to perform statistical analysis. Canonical Correlation Analysis (CCA) is a generalization of the concept of correlation between two variables for finding patterns of maximum correlation between two sets of variables (Von Storch and Zwiers, 1999, Sec. 14). If $\overrightarrow{x} = [x_1, ..., x_k]$ and $\overrightarrow{y} = [y_1, ..., y_l]$ are the two sets of variables, CCA finds the optimal linear combinations $u = \sum_{i=1}^{k} a_i x_i$ and $v = \sum_{j=1}^{l} b_j y_j$, such that the correlation between the canonical variates u and v is maximized.

In our case, $\overrightarrow{x}$ consists of the leading principal components (PCs) extracted from a principal component analysis (PCA) of the monthly Line-P temperature data set, after removal of the seasonal cycle at each point. Each PC x_i is therefore associated with a spatial pattern, and u also represents the temporal variation of a mode, later referred to as the Line-P CCA mode. A regular PCA is not possible for our Line-P data set since it contains too many gaps. We used an alternative method which handles gappy data (Von Storch and Zwiers, 1999, Sec. 13.2.8). Hence, the PCA extracts the main variations of Line-P anomalies, reduces the noise (trapped in secondary PCs), and also gives non-gappy time series for the CCA.

The number of Line-P PCs to be used in the CCA has to be large enough to include small variability that may be associated with a given mechanism, but our data set also contains

much noise, which may appear even in the leading modes. We used 9 PCs for Line-P temperature anomalies (representing 63% of the total variance), the variance explained by the 10th PC being significantly lower than the variance explained by the previous modes (not shown). In any case, the results of this study do not change much when adding more PCs, with only increased noise in the spatial patterns.

The second input set of variables $\overrightarrow{y}$ has to account for the main anomaly variations of the forcing mechanism considered. In the case of forcing mechanisms directly acting over the surface of the ocean, it consists of the 3 leading PCs of proxy variables and v is also associated with a spatial pattern. The PCA is performed for the same period of time as for the Line-P PCs (May 1956 - September 2002) over the domain directly overlying Line-P: $[47.5^o\text{N}; 52.5^o\text{N}] \times [125^o\text{W}; 145^o\text{W}]$ (3×9 points). The number of spatial points is small, which explains the use of only 3 PCs to account for the main variability over this domain. Also, adding more PCs does not change the results significantly. In the case of remote or localized forcing mechanisms, a proxy is averaged over a specific region to form an index, and the result of the CCA is the Line-P mode that is most correlated with this index.

All the input time series used for the CCA have been smoothed using a three-month running mean. Also, if we perform the CCA with all frequencies included in the input time series, long-term oscillations might explain most of the correlation found and in fact correspond to indirect broad scale variations (such as PDO). To get the modes of maximum correlation for variations with periods ranging between a few months to a few years, we subtracted the five-year running mean from all input time series. The CCA then finds the two combinations for the two sets of variables which give the highest correlation only with respect to the higher frequencies of the input time series. The two combinations of variables found by the CCA (with only high frequencies considered) are then applied

to the original time series (low frequencies included) to get the real temporal variations of the CCA modes, which eventually contain interdecadal oscillations. Actually, if the Line-P temperature anomaly mode was totally determined by the forcing anomaly mode, the variations of the two modes would also match for low frequencies, even if only high frequencies were used in the CCA. Nevertheless, since the Line-P mode always captures extra variability not directly accounted by the forcing considered, it is useful to consider how the two CCA time series match for low frequencies when nothing has been done to correlate them. This may help in seeing if the Line-P mode captures variability not accounted for by the forcing mode.

Time lags, ranging from -20 to +20 months, have also been applied between the two input sets of variables before performing the CCA, in order to determine the timing of maximum CCA correlation. Line-P response to the forcing is then considered and studied for this lag. A comparison between the CCA correlations found around zero-lag (when we expect to find the response, hence the highest correlations) and the correlations at large lags (when low correlations are expected) helps in considering the relevance of the results. Nevertheless, a more objective test is also used.

To test if a correlation is significant, we compute random normally distributed time series, with the same variance as the actual ones used, and perform 1000 equivalent CCAs. We can then consider the percentage of random CCAs giving lower correlations than the correlation found from the study, which gives an idea of the significance of the mode.

As the original time series are autocorrelated, the effective sample size is not the total length of the data. We use the first zero crossing method to determine the effective sample size. The first lag l_0 for which the autocorrelation coefficient reverses sign gives an autocorrelation time scale. A crude estimation of the effective sample size is then $N_{eff} = N/l_0$,

where N is the number of points in the original time series. N_{eff} is different for each time series but we need only one value to generate the random tests. For each forcing mechanism studied, we used the mean effective sample size of all CCA input time series (Line-P and forcing ones) for the 1000 random CCA runs.

2.2.2 Method Limitation

The CCA method only exhibits simple and direct relationships between the two input sets of variables. The approximation is that the forced field at a given time $u(t)$ (Line-P temperature anomalies in our case) is considered to be directly related to the forcing field also at a fixed time (although potentially lagged) $v(t-l)$. Nevertheless, in the real world the ocean acts as a low pass filter that for instance integrates the atmospheric white noise to produce a reddened ocean response (Hasselmann, 1976). A simple form of equation that allows for this integration is the stochastic climate model (Frankignoul and Hasselmann, 1977):

$$\frac{d\theta}{dt} = F - \lambda\theta,$$

where θ represents an oceanic variable (for example SST), F the atmospheric forcing and λ^{-1} the time scale of the oceanic response that may be determined from lagged autocorrelations. The approach in our paper is consistent with assuming the time scale of the oceanic response being sufficiently short so that the time derivative in the above equation can be ignored, and the ocean temperature becomes directly proportional to the forcing. This assumption might be reasonable for mechanisms that have a short response time like coastal upwelling, but is more doubtful for open water processes for which λ^{-1} is usually estimated to 1-2 years from different oceanic variables (e.g. from isopycnal displacement in Cummins and Lagerloef, 2002). It should therefore be kept in mind that only fast-responding processes

are likely to be well captured in this study.

3 Results

3.1 Ekman transport

When a steady wind stress is applied to the surface of the ocean, a depth-integrated transport flows 90^o to the right of the stress in the North Hemisphere (Gill, 1982):

$$\overrightarrow{U_E} = \frac{\overrightarrow{\tau} \times \overrightarrow{k}}{\rho f} \tag{1}$$

where $\overrightarrow{U_E}$ is the Ekman transport, $\overrightarrow{\tau}$ the wind stress, $\overrightarrow{k}$ the vertical unit vector (pointing upward), ρ the density of the water, f the Coriolis parameter.

We expect temperature anomalies in the Ekman layer to be proportional to the strength of the Ekman transport anomalies and the temperature gradient along the direction of the transport:

$$T_{ET}^{(a)}(\alpha) \propto -U_{E\alpha}^{(a)} \partial T / \partial X_{\alpha - 90} \tag{2}$$

where superscripts (a) refer to anomalies, $T_{ET}^{(a)}(\alpha)$ represents the temperature anomalies found in the Ekman layer for a wind stress applied in the direction α, $U_{E\alpha}^{(a)}$ the Ekman transport anomalies associated with it, $\partial T / \partial X_{\alpha - 90}$ the horizontal temperature gradient in the direction $\alpha - 90^o$.

Taking the time derivative into account, the equation of motion in the Ekman layer becomes:

$$\frac{\partial \overrightarrow{U_E}}{\partial t} + f \overrightarrow{k} \times \overrightarrow{U_E} = \frac{1}{\rho} \overrightarrow{\tau} \tag{3}$$

and we can expect slightly different behaviors than in the case of steady motion. Especially, considering an oscillatory wind stress applied at the surface of the ocean $\overrightarrow{\tau} = \overrightarrow{\tau_a} e^{i\omega t}$ and looking for solutions with the same frequency $\overrightarrow{U_E} = \overrightarrow{U_{Ea}} e^{i\omega t}$, the equation becomes:

$$i\omega \overrightarrow{U_{Ea}} + f \overrightarrow{k} \times \overrightarrow{U_{Ea}} = \frac{1}{\rho} \overrightarrow{\tau_a} \tag{4}$$

and we can expect a phase shift between the Ekman transport and the applied wind stress.

We have studied the effect of an applied wind stress over Line-P in the zonal and the meridional directions separately. Anomalies are calculated for the region $[47.5^o\text{N}; 52.5^o\text{N}] \times [125^o\text{W}; 145^o\text{W}]$. The first three PCs used for the CCA are calculated for the same period as for Line-P data (May 1956 - September 2002).

For the zonal wind stress anomalies, the highest correlation is found for Line-P temperature anomalies lagging wind stress anomalies by +2 months (Fig. 2a). This peak in correlation around zero-lag indicates that the two signals are significantly correlated, which is also confirmed by the test (see the table in Fig. 2). The forcing CCA spatial pattern (Fig. 2b) indicates positive zonal (ie westerly) wind stress anomalies over the whole domain with a strong gradient in the offshore direction. The Line-P CCA spatial pattern (Fig. 2c) consists of negative temperature anomalies concentrated in the upper layer and spread all along Line-P. Their strength decreases regularly with depth and are almost null around 150 m. At station 1 (0 km along Line-P, 35 km from the coast), very strong anomalies are present up to 100 metre-depth. The correlation of the two time series is lower when the long-term variations are added. The Line-P mode has a strong low-frequency signal,

contrary to the forcing CCA time series (Fig. 2d).

The negative sign of the Line-P surface temperature anomalies associated with positive zonal wind stress anomalies is consistent with anomalous advection of cooler water from the north as expected from Ekman theory. Nevertheless, strong offshore increase in the magnitude of the forcing anomalies along Line-P do not correspond to a similar increase in the surface temperature anomalies. For a given zonal wind stress anomaly over Line-P, the surface temperature anomalies should be greater in the case of a stronger mean meridional temperature gradient. Thus the meridional surface temperature gradient may be decreasing in strength inversely to the applied zonal wind stress anomalies in the offshore direction.

We averaged long-term mean (Levitus) ocean temperature from the surface to 20 m depth and derived the meridional temperature gradients. In Fig. 3a, the gradient gets weaker (absolute value) from the coast to around 134^{o}W, ranging from -4.5 to nearly $-2.5^{\mathrm{O}}C/1000$ km. From 134^{o}W to 145^{o}W, there is a slight trend towards stronger gradients. From the coast to 135^{o}W, the strong increase in zonal wind stress anomalies (Fig. 2b) is associated with a significant decrease in the strength of the meridional surface temperature gradient. From 135^{o}W to 145^{o}W, the two fields are almost constant in magnitude. This relationship is consistent with the weak spatial variability of surface temperature anomalies observed along Line-P. The depth over which large temperature anomalies occur (around 100 m depth) is consistent with typical Ekman layer depth, usually thought to be between 10 and 100 m deep (Gill, 1982). As the coast of Vancouver Island is roughly directed northwestward, the positive zonal wind stress anomalies have an alongshore component directed southeastward which can lead to anomalous upwelling around station 1.

The highest CCA correlation found for a lag of +2 months suggests a phase shift between the wind stress and the resulting Ekman transport. The long-term variations of the Line-P

time series, not found in the forcing series, suggest that another mechanism influences the low-frequency variability of the surface temperature along Line-P.

For the meridional wind stress anomalies, a peak in the canonical correlation appears at a lag of +1 month (Fig. 4), significant at 94%. The forcing CCA spatial pattern indicates positive anomalies over the whole domain, with the strongest ones being found between 130^oW and 135^oW. The corresponding Line-P CCA pattern consists of weak negative surface temperature anomalies farther than 400 km along Line-P (west of 130^oW) and strong nearshore positive anomalies. The nearshore anomalies extend down to 100 m depth and are centered 100 km from station 1 at approximately 30 m depth.

From Ekman theory, the meridional wind stress anomalies induce zonal transports. To interpret the surface temperature anomalies observed in the Line-P CCA mode, we calculated the mean zonal surface temperature gradient along Line-P (Fig. 3b). From around 130^oW to 145^oW, the zonal temperature gradient is positive, associated with warmer temperature in the eastward direction. Positive meridional wind stress anomalies are expected to result in anomalous eastward transport, leading to negative temperature anomalies for this section of Line-P, as observed in the Line-P CCA spatial pattern (Fig. 4c). The strongest forcing anomalies found between 130^oW and 135^oW are associated with moderate zonal temperature gradients, compared to farther offshore, which can explain the small variability of the surface anomalies in this region. East of 129^oW, the zonal surface temperature gradient is negative, and positive meridional wind stress anomalies should lead to positive surface temperature anomalies, as is actually observed. The location of the transition between negative and positive temperature anomalies around 400 km along Line-P is well explained by the change in the sign of the mean zonal temperature gradient.

Close to the coast, the temperature anomalies result from a coastal effect of the wind

stress. Positive meridional wind stress anomalies along the coast result in downwelling anomalies, which influence the coastal currents. This effect is studied in more detail later.

The two time-series are less well correlated for the long-term variations, where the low-frequency signal is large for the Line-P mode, but not for the forcing time series.

3.2 Wind mixing

Wind speed affects the rate of mixing of the ocean surface layer, energy arguments suggest that the rate of deepening of the mixed layer (rate of gain of potential energy) might be related to the cube of the wind speed (the rate at which work is done on the sea surface). Positive wind speed anomalies are expected to be associated with negative temperature anomalies in the surface layer; meanwhile, as warmer surface waters are mixed down, positive temperature anomalies are also expected near the bottom of the mixed layer.

To test if we can get higher correlations for wind speed cube anomalies, we examined the highest CCA correlation between 0 and 3-month lag for different powers of the wind speed, and found that the correlation dropped for powers greater than 1 (not shown). We suspect that with increasing powers, the noise gets amplified compared to the signal, which results in lower correlations. Hence we will only consider anomalies of the wind speed, i.e. with the power equal to 1.

A peak in correlation occurs for a lag of +2 months (Fig. 5), significant at 95%. The forcing CCA spatial pattern consists of positive anomalies centered around 140^oW south of Line-P. Close to the coast (East of 130^oW), the wind speed anomalies are very weak. For the Line-P CCA spatial pattern, the temperature anomalies appear at the surface all along Line-P. In the far offshore section (farther than 1100 km along Line-P), the surface variability is the strongest of all and anomalies extend down to 100 m with a relatively

smooth decrease. In the intermediate section (300 to 1100 km along Line-P), the anomalies are concentrated in the upper 40 m. The nearshore section (0 to 300 km) has weak negative anomalies near the surface and weak positive ones below.

The negative sign of the surface temperature anomalies associated with positive wind speed anomalies is consistent with enhanced mixing with colder deeper water. The spatial variation in the strength of the surface temperature anomalies is also consistent with the variations in the strength of the overlying wind speed anomalies. The strongest ones are found far offshore and the anomalies are very weak in the nearshore domain. The different depths of the anomalies in the three domains tend to follow the climatological mixed layer depth (Laîné, 2004, Fig. 3.6), which is much shallower nearshore.

3.3 Upwelling and downwelling

Northward (southward) alongshore winds lead to onshore (offshore) Ekman transports, which result in accumulation (depletion) of surface water at the coast, thus leading to coastal downwelling (upwelling). Stronger (weaker) upwelling implies cold (warm) anomalies in the upper layer close to the coast associated with more (less) cold deep water being upwelled. Oppositely, stronger (weaker) downwelling is expected to result in positive (negative) temperature anomalies. Thus, northward alongshore wind stress anomalies should result in positive temperature anomalies at the coast, although the relationship might not be linear and the depth of the temperature anomalies might also be a function of the actual upwelling or downwelling context.

Apart from the direct effect of upwelling anomalies, another associated process is also expected to change the temperature field at the coast through anomalous coastal currents. Anomalous upwelling (downwelling) rates cause the surface height to drop (rise) slightly, the

pycnoclines to rise (drop), and subsequent northward coastal current anomalies in the upper layer to be negative (positive) through geostrophic adjustment. Finally, coastal current anomalies result in a displacement of the mean alongshore temperature gradient. Therefore, positive coastal temperature in the upper layer are also expected from northward alongshore wind stress anomalies through current anomalies.

The alongshore wind stress near the coast at Line-P is computed from the average of alongshore wind stress components at 6 locations surrounding the west coast of Vancouver Island (Fig. 1). Since there is some uncertainty in the alongshore direction, CCA was computed using the wind stress component rotated at various angles, counterclockwise from the alongshore direction. The highest canonical correlation was found for a rotation of 15^o and a lag of +1 month (Fig. 6).

As expected, the main variability occurs near the coast. Two main positive anomaly centers are found, with the first down to 100 m at station 1 (0 km along Line-P, 35 km from the coast), and the second around 30 m depth at station 3 (87 km from station 1, 70 km from the coast). The temperature anomalies decrease down to 300 m along the continental slope, and farther offshore to a little beyond 100 m. Line-P time series contains strong low-frequency signals compared to the forcing, but the long-term oscillations are synchronized for most periods between the two.

The observed positive coastal temperature anomalies are expected for northward alongshore wind stress. We see downwelling effects from the deep strong anomalies found at Station 1, by the accumulation of warm surface water at the coast and enhanced northward coastal current. The broader variability, centered at station 3 may correspond to northward advection anomalies by the broader coastal current.

3.4 Perturbations along the west coast of North America

Advection anomalies for the entire California Current can lead to temperature anomalies found along Line-P, as has been suggested as an explanation for the 2002 anomalies (Barth, 2003; Kosro, 2003). Northward coastal current anomalies result in a northward displacement of the mean temperature gradient at the coast, thus leading to positive temperature anomalies at the coast in the upper layer (see Sec. 3.3).

The displacement of isopycnals and sea surface height (SSH) associated with alongshore wind stress anomalies, responsible for the coastal current anomalies through geostrophic adjustment at a given location, can also propagate northward as coastally trapped waves. Those waves can reach Line-P and lead to temperature anomalies (especially around the usual depth of the permanent thermocline) due to isopycnal perturbations.

We studied Line-P temperature anomalies resulting from perturbations from the south (coastal current anomalies and coastal wave propagation) by using SSH anomalies at Crescent City as an input time series for the CCA. Crescent City is located in Northern California and sea levels have been recorded before our first available data for Line-P. The data set is very complete and was made available through a web page courtesy of the NOAA Center for Operational Oceanographic Products and Services. We converted the hourly time series into a monthly time series by first applying a 29.5 days running mean to remove the lunar fortnightly tide (14.77 days period), then averaging the values in a given month.

Fig. 7 shows the peak correlation at a lag of +1 month. The Line-P CCA spatial pattern indicates strong positive anomalies at station 1 down to 100 m. These anomalies extend westward along Line-P in the upper 100 m with decreasing strength. Weakening anomalies are also observed over the continental slope down to 450 m. The far offshore domain also includes moderate positive temperature anomalies down to 200 m. Line-P mode and the

forcing time series contain similar interannual to decadal oscillations, even if the correlation decreases from 0.63 to 0.56 when interdecadal oscillations are included.

The sign of Line-P temperature anomalies is consistent with the expected physics. Positive SSH anomalies should indeed be associated with northward coastal current anomalies and a situation where isopycnals are anomalously deep, thus positive temperature anomalies (accumulation of warm water at the coast). The positive temperature anomalies along Line-P come from the northward displacement of the mean alongshore temperature gradient due to coastal current anomalies and the northward propagation of perturbations as coastal waves. The latter phenomena can also be seen from the deep extension of temperature anomalies over the continental slope. Most of the SSH anomalies at Crescent City result from local alongshore wind stress anomalies, which is suggested by similar results obtained by the CCA performed with alongshore wind stress anomalies averaged over the west coast of the United States (not shown). The Crescent City sea level anomalies also include anomalies originating farther south, especially coastal waves propagating from the tropics during strong El Niño events, as indicated by the strong positive anomalies found during several El Niño events (in particular during the winters of 1957/1958, 1982/1983, 1991/1992, 1992/1993 and 1997/1998) and negative anomalies during several La-Niña events (1956/1957, 1963/1964, 1970/1971, 1974/1975, 1984/1985 and 1988/1989).

The interannual to decadal Line-P oscillations are well explained by the forcing time series (Fig. 7c). Although the correlation decreases when the 5-year running mean is included, it is only due to a nearly 50-year period oscillation in the Line-P time series (with lower values before 1978 and higher after 1978), which is missing in the forcing time series, creating an offset for the decadal oscillations. Thus, the yearly to decadal oscillations in the Line-P mode can be explained by a remote influence from the south, mostly associated

with ENSO events.

3.5 Other mechanisms and discussion

Laîné (2004) also studied various other forcing mechanisms for Line-P temperature anomalies. However, he found either insignificant correlations or significant correlations but with the sign and/or distribution of anomalies disagreeing with the physics expected from the mechanism considered. These unsuccessful studies include:

- Wind stress curl anomalies over Line-P to account for Ekman pumping or Sverdrup balance anomalies;
- Net sensible and latent heat flux anomalies over Line-P;
- Clear sky downward solar and long-wave flux anomalies over Line-P to account for anomalous atmospheric conditions;
- Net cloud forcing solar and long-wave flux anomalies over Line-P to account for cloud effects on radiation;
- Advection of temperature anomalies along the North Pacific Current (input forcing time series being the average of SST anomalies over the domain west of Line-P $[48^o\text{N}; 52^o\text{N}] \times [160^o\text{W}; 170^o\text{W}]$);
- Alaska Current anomalies derived from alongshore wind stress anomalies along the eastern margin of the Gulf of Alaska.

These results are not shown in this paper but can be found in Laîné (2004). Pickett and Paduan (2003) showed the strong influence of Ekman pumping on coastal upwelling in the

California Current System. Murphree et al. (2003) also indicates that seasonal variations of the wind stress curl strongly impact the upper ocean temperature along most of the NEP eastern margin. Farther offshore, Cummins and Lagerloef (2002) found that a large fraction of the pycnocline variability at Ocean Station Papa (last station of Line-P) can be explained by the local Ekman pumping forcing. In fact, the discrepancy with our results, for which no significant correlations could be found between wind stress curl anomalies and Line-P upper layer temperature anomalies, is probably due to the non-integration of the atmospheric forcing in our method (see Sec. 2.2.2), contrary to the study of Cummins and Lagerloef, where a simple stochastic model had been used to integrate the atmospheric forcing before applying the CCA.

Note also that this non-integration limitation consists of an approximation for the results found for other forcing as well, even when significantly correlated and physically consistent. Indeed, the role of Ekman transport on upper-ocean temperature anomalies for example should also be integrated; the advection of the mean gradient is obviously stronger after two months of positive zonal wind stress anomalies than after one month of negative anomalies followed by one month of positive anomalies. As already discussed in Sec. 2.2.2, our technique is probably only suitable for capturing fast-responding processes.

Hence, the influence of other mechanisms might also have a role in determining temperature anomalies in the NEP. It may explain why no forcing is found responsible for the low-frequency signal of offshore temperature anomalies along Line-P and why only a small part of the total variance of Line-P temperature anomalies can be explained by a given mechanism. Finally, the results of this study should be considered as an analysis of the mean anomalous mechanisms acting on temperature anomalies in the NEP. When analyzing a specific situation, like the 2002 anomalies (see Introduction), we also need to consider

the interactions between the different mechanisms, ie. the setting of anomalous conditions by a given mechanism at a given time followed by another forcing anomaly etc. Those interactions are not explicitly taken into account in our study.

4 Conclusions

In this section, we will consider the different spatial domains along Line-P, and present the dominant forcing mechanisms for each. The two domains are the offshore section of Line-P (farther than 400 km along Line-P, or 225 km from shore) and the coastal section (as far as 300 km along Line-P or 180 km from shore).

4.1 Offshore domain

The only forcing mechanisms for which the offshore temperature anomalies were consistent with the forcing anomalies, were the Ekman transport due to the zonal and meridional wind stress, and wind mixing. In the case of zonal wind stress anomalies, the strength of the forcing anomalies found over the region and the variability of the mean meridional surface temperature gradient could explain the strength of the observed temperature anomalies. The deepest depth to which temperature anomalies could be found was consistent with an Ekman layer of the order of 100 m. In the case of wind mixing, the strength of wind speed anomalies was strong over the domain, and the depth of the temperature anomalies was consistent with typical mixed layer depths. For meridional wind stress anomalies, the strength of the observed ocean temperature anomalies was significantly smaller than for the previous two processes.

It may be impossible to know if one of the two supposedly most influential mechanisms

(Ekman transport due to zonal wind stress anomalies and wind mixing) has a stronger influence compared to the other one, especially since the two CCA correlations are of the same order (0.50 and 0.46 for zonal wind stress anomalies and for wind speed anomalies, respectively). Also, the correlation between the two forcing CCA time series is significant (0.53, low frequencies removed), which indicates that the mechanisms partly occur simultaneously, making any statistical attempt to distinguish their roles futile. Nevertheless, the Line-P CCA spatial patterns are different for the entire domain in the two studies (Figs. 2c and 5c), which suggests that the modes do not capture exactly the same variability. Also, since the spatial distribution of the anomalies was consistent with the forcing considered in each case, the two Line-P modes seem to represent the influence of each mechanism over the entire domain, and especially for the offshore section of Line-P.

4.2 Coastal domain

Coastal anomalies were significantly strong and consistent with the results expected when the forcing anomalies were derived from zonal and meridional wind stress (Sec. 3.1), upwelling/downwelling favourable wind stress along the coast of Vancouver Island (Sec. 3.3) and SSH at Crescent City (Sec. 3.4). The influence of zonal and meridional wind stress anomalies over nearshore temperature anomalies is included in the study of coastal upwelling and downwelling.

For the two remaining most influential mechanisms (coastal upwelling/downwelling and perturbations along the coast of North America), we suspect that the two influences strongly overlap. Indeed, during strong ENSO events, alongshore wind anomalies offshore Vancouver Island could be related to alongshore wind anomalies farther south, and/or coastal wave propagation from the tropics (see Introduction). In fact, SSH anomalies at Crescent City and

alongshore wind stress anomalies offshore Vancouver Island are not significantly correlated (0.36), which suggests that the two distinct influences can be captured. Although the two Line-P spatial patterns look similar (which is expected from a coastal influence of both mechanisms), some distinct features (an anomaly center around 70 km along Line-P in Fig. 6b and a deeper extension of anomalies along the continental slope in Fig. 7b) suggest that the separate influences are indeed captured by our CCA and that both mechanisms are important. We conclude that the dominant mechanisms responsible for temperature anomalies as far as 180 km from the coast are coastal upwelling and downwelling (wind stress anomalies along Vancouver Island coast) and anomalous conditions farther south (involving coastal current anomalies and/or propagation of coastal waves).

Comparing the long-term oscillations of forcing and Line-P temporal coefficients indicates that Line-P decadal oscillations are mostly associated with coastal phenomena. Coastal upwelling and downwelling anomalies have similar interannual to decadal oscillations as the associated Line-P mode (despite a smaller amplitude, Fig. 6c), as do SSH anomalies at Crescent City and its associated temperature anomalies along Line-P (despite a multidecadal oscillation in the Line-P mode not found in the forcing time series, Fig. 7c). Those oscillations are mostly related to ENSO events (Sec. 3.4).

4.3 Perspectives

The inability of our study to detect the influence of Ekman pumping anomalies on upper ocean temperature despite the results of earlier studies is probably due to a limitation of our method which does not integrate the forcing over time. Ekman pumping process, along with other mechanisms (especially in the offshore domain) may not have been extracted because of the slow oceanic response associated with them (Sec. 2.2.2). It can also explain why we

did not find any forcing mechanisms associated with a nearly 50-year oscillation of upper ocean temperature anomalies in the NEP. The next step would be to use an ocean model to first integrate the atmospheric forcing before applying CCA to find relations between the outputs of this model and the Line-P PCs, as in Lagerloef (1995).

It is also interesting to note the use that can be made of hydrographical line surveys through the use of PCA. It indeed gives monthly data of a complete oceanic transect from samples originally much sparser in time and space. Also not initially obvious is the fact that the information contained in the leading PCs is relevent despite the highly gappy original data sets. It can thereafter be used to perform statistical analysis as illustrated in this study.

Acknowledgments

A. Laîné is grateful to Drs. Susan Allen and Richard Pawlowicz for their helpful comments on his M.Sc. thesis, from which this paper is based. Special acknowledgments should also be made to the reviewers of the paper for their many helpful remarks that made this article more readible and more complete. This work is supported by a science academic subvention from the Department of Fisheries and Oceans and a discovery grant from the Natural Sciences and Engineering Research Council of Canada.

References

[1] Barth J.A. (2003). Anomalous southward advection during 2002 in the northern California Current: Evidence from Lagrangian surface drifters. *Geophysical Research Letters*, 30(15): 8024, doi:10.1029/2003GL017511

[2] Beaubien E.G. and Freeland H.J. (2000). Spring phenology trends in Alberta, Canada: Links to Ocean Temperature, *International Journal of Biometeorology*, 44(2): 53-59

[3] Chavez F.P., Ryan J., Lluch-Cota S.E., Niquen M.C. (2003). From anchovies to sardines and back: Multidecadal Change in the Pacific Ocean. *Science*, 299: 217-221

[4] Cummins P.F. and Lagerloef G.S.E. (2002). Low-frequency pycnocline depth variability at Ocean Weather Station P in the northeast Pacific. *Journal of Physical Oceanography*, 32: 3207-3215

[5] Enfield D.B. and Allen J.S. (1980). On the structure and dynamics of monthly mean sea level anomalies along the Pacific coast of North and South America. *Journal of Physical Oceanography*, 10: 557-578

[6] Frankignoul C. and Hasselmann K. (1977). Stochastic climate models, Part II: Application to sea-surface temperature anomalies and thermocline variability. *Tellus*, 29: 289-305

[7] Freeland H.J., Gatien G., Huyer A. and Smith R.L. (2003). Cold halocline in the northern California Current: An invasion of Subarctic water. *Geophysical Research Letters*, 30(3), 1141, doi: 10.1029/2002GL016663

[8] Gill A.E. (1982). Atmopshere-Ocean Dynamics. International Geophysics Series, volume 30. Academic Press.

[9] Hasselmann, K. (1976). Stochastic climate models, Part I: Theory. *Tellus*, 28: 473-485

[10] Hsieh W.W. and Tang B.Y. (2001). Interannual variability of accumulated snow in the Columbia basin, British Columbia. *Water Resources Research,* 37: 1753-1760

[11] Hsieh W.W., Tang B.W. and Garnett E.R. (1999). Teleconnections between Pacific sea surface temperatures and Canadian prairie wheat yield. *Agricultural and Forest Meteorology*, 96: 209-217

[12] Hsieh W.W., Yuval J.L., Shabbar A. and Smith S. (2003). Seasonal prediction with error estimation of Columbia River streamflow in British Colombia. *Journal of Water Resources Planning and Management*

[13] Huyer A. and Smith R.L. (1985). The signature of El Nino off Oregon, 1982-1983. *Journal of Geophysical Research*, 90: 7133-7142

[14] Huyer A. (1980). The offshore structure and subsurface expression of sea level variations off Peru 1976-1977, *Journal of Physical Oceanography*, 10: 1755-1768

[15] Kawasaki T. (1983). Why do some pelagic fishes have wide fluctuations in their numbers? - biological basis of fluctuation from the viewpoint of evolutionary ecology. *FAO Fish. Rep.,* 291 (2, 3): 1065-1080

[16] Kosro P.M. (2003). Enhanced southward flow over the Oregon shelf in 2002: A conduit for subarctic water. *Geophysical Research Letters*, 30(15): 8023, doi:10.1029/2003GL017436

[17] Lagerloef G.S.E. (1995). Interdecadal variations in the Alaska Gyre. *Journal of Physical Oceanography*, 25: 2242-2258

[18] Laîné A. (2004). Forcing Mechanisms Controlling Surface and Subsurface Temperature Anomalies along Line-P, Northeast Pacific Ocean. M.Sc. thesis, University of British Columbia, 80 pp.

[19] Lluch-Belda D., Crawford R.J.M., Kawasaki T., MacCall A.D., Parrish R.H., Schwartzlose R.A. and Smith P.E. (1989). World-wide fluctuations of sardine and anchovy stocks: the regime problem. *South African Journal of Marine Science*, 8: 195-205

[20] Mantua N.J., Hare S.R., Zhang Y., Wallace J.M. and Francis R.C. (1997). A Pacific Interdecadal Climate Oscillation with Impacts on Salmon. *Bulletin of the American Meteorological Society,* 78 (6): 1069-1079

[21] McKinnell S., Freeland H.J. and Groulx S.D. (1999). Assessing the northern diversion of sockeye salmon returning to the Fraser River, B.C. *Fisheries Oceanography,* 8: 104-114

[22] Murphree T., Bograd S.J., Schwing F.B. and Ford B. (2003). Large-scale atmosphere-ocean anomalies in the Northeast Pacific during 2002. *Geophysical Research Letters*, 30(15): 8026, doi:10.1029/2003GL017303

[23] Pickett M.H. and Paduan J.D. (2003). Ekman transport and pumping in the California Current based on the U.S. Navy's high-resolution atmospheric model (COAMPS). *Journal of Geophysical Research*, 108: 3327, doi:10.1029/2003JC001902

[24] Qiu B. (2002). Large-scale variability in the midlatitude subtropical and subpolar North Pacific Ocean: Observations and causes. *Journal of Physical Oceanography*, 32: 353-375

[25] Royer T.C. (1981). Baroclinic transport in the Gulf of Alaska, Part II. A fresh water driven coastal current. *Journal of Marine Research*, 39: 251-266

[26] Schwing F.B., Murphree T., deWitt L., Green P.M. (2002). The evolution of oceanic and atmospheric anomalies in the northeast Pacific during the El Nino and La Nina events of 1995-2001. *Progress in Oceanography*, 54: 459-491

[27] Simpson J.J. (1984). El Nino-induced onshore transport in the California Current during 1982-1983. *Geophysical Research Letters*, 11: 133-236

[28] Strub P.T. and James C. (2002a). Altimeter-derived surface circulation in the large-scale NE Pacific gyres: Part 1. Seasonal variability. *Progress in Oceanography*, 53(2-4): 163-183

[29] Strub P.T. and James C. (2002b). Altimeter-derived surface circulation in the large-scale NE Pacific gyres: Part 2. 1997-1998 El Nino anomalies. *Progress in Oceanography,* 53(2-4): 185-1214

[30] Strub P.T. and James C. (2003). Altimeter estimates of anomalous transports into the California Current during 2000-2002. *Geophysical Research Letters*, 30(15): 8025, doi:10.1029/2003GL017513

[31] Von Storch H. and Zwiers F.W. (1999). Statistical Analysis in Climate Research. Cambridge University Press.

[32] Whitney F.A. and Freeland H.J. (1999). Variability in upper-ocean water properties in the NE Pacific Ocean. *Deep-Sea Research II,* 46: 2351-2370

List of Figures

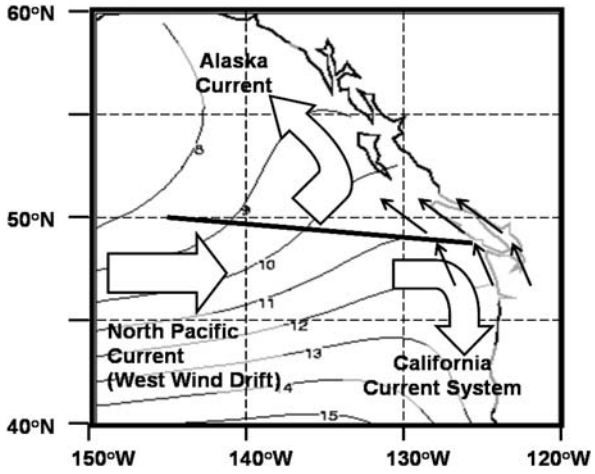

Figure 1: Map showing the location of Line-P; the location and direction of the alongshore wind stresses used to derive the upwelling/downwelling index (thin arrows); a simplified sketch of the currents (large arrows) and the climatological SST (Levitus) found in the NEP.

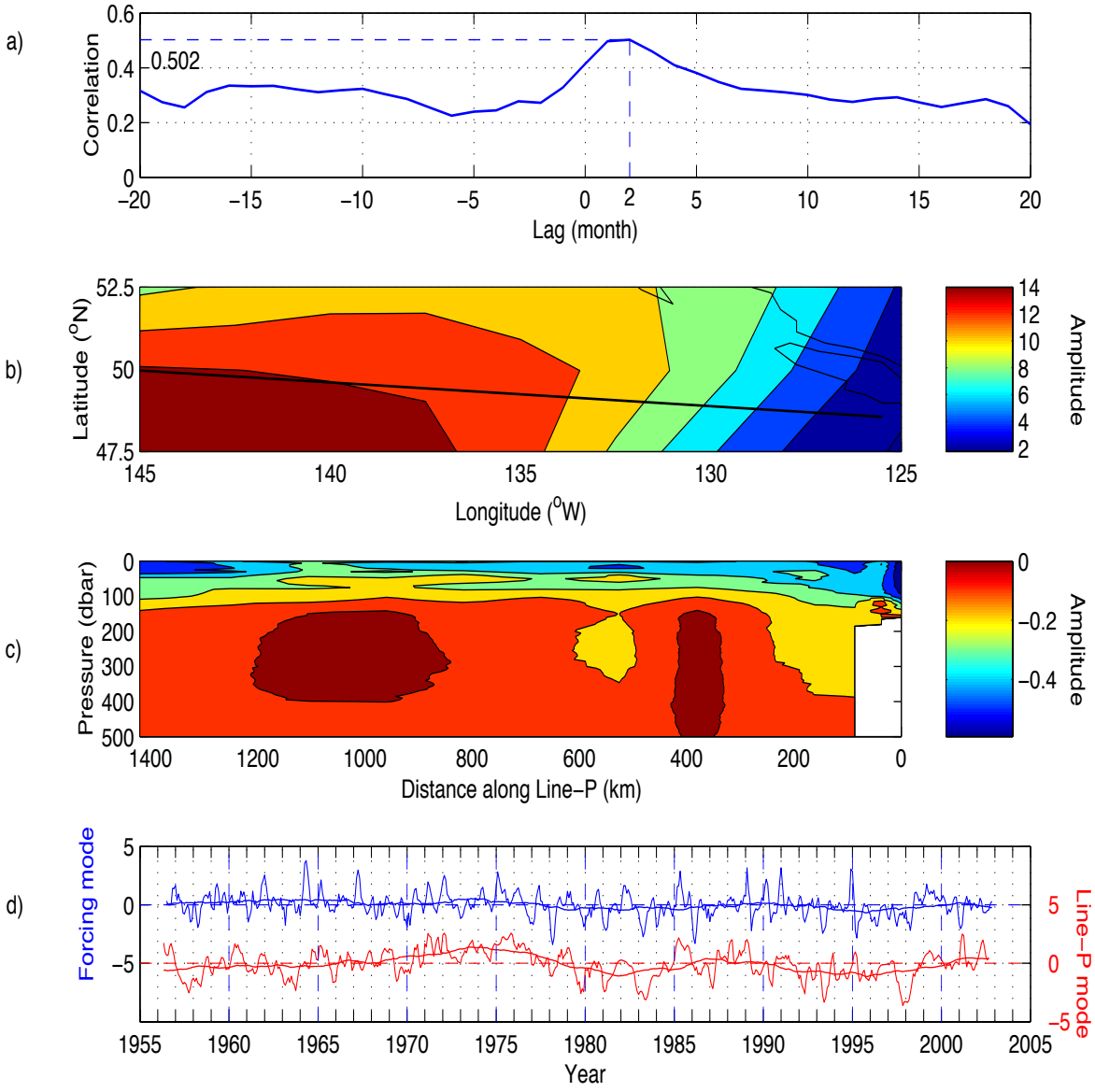

Lag (month)	Variance explained 1	Variance explained 2	Correlation 1	Correlation 2	Significance test
+2	76.8%	12.4%	0.50	0.47	99.2%

Figure 2: CCA between 3 PCs of zonal wind stress anomalies over Line-P ($[47.5^oN; 52.5^oN] \times [125^oW; 145^oW]$) and 9 PCs of Line-P temperature anomalies. **a)** CCA correlations with lags, positive lag means Line-P temperature lagging the forcing; **b)** Forcing CCA spatial pattern; **c)** Line-P CCA spatial pattern; **d)** Standardized CCA temporal coefficients (with the five-year running means shown) for the forcing CCA mode (top) and the Line-P CCA mode (bottom) (year ticks correspond to January for the Line-P mode time series). The table gives the **lag** considered; **Variance explained 1** is the variance explained by the forcing CCA mode, **Variance explained 2** by Line-P CCA mode; **Correlation 1** is the CCA correlation (5-year running mean removed from CCA-input variables), **Correlation 2** is the correlation between the two CCA modes shown in d) (all frequencies included); **Significance test** is the percentage of random CCA giving a lower correlation than correlation 1.

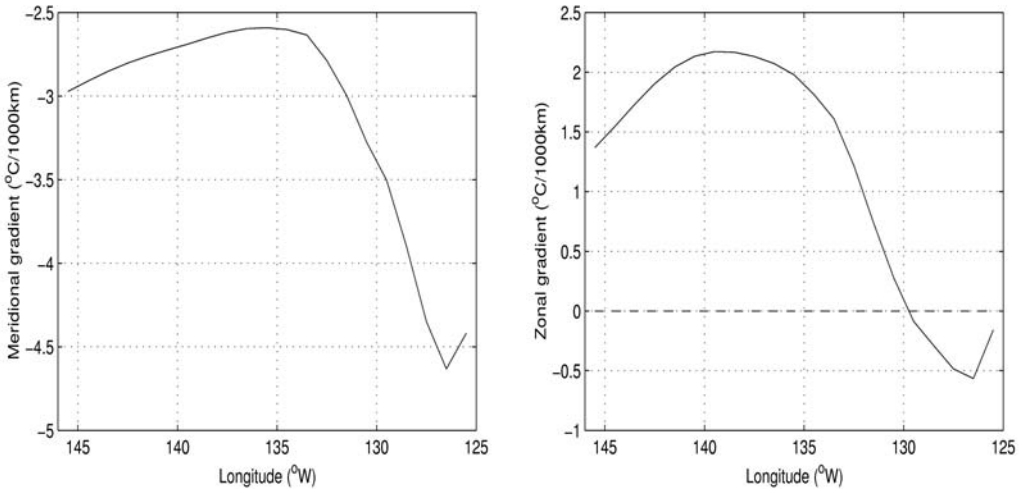

(a) (b)

Figure 3: Mean (a) meridional and (b) zonal surface temperature gradient along Line-P.

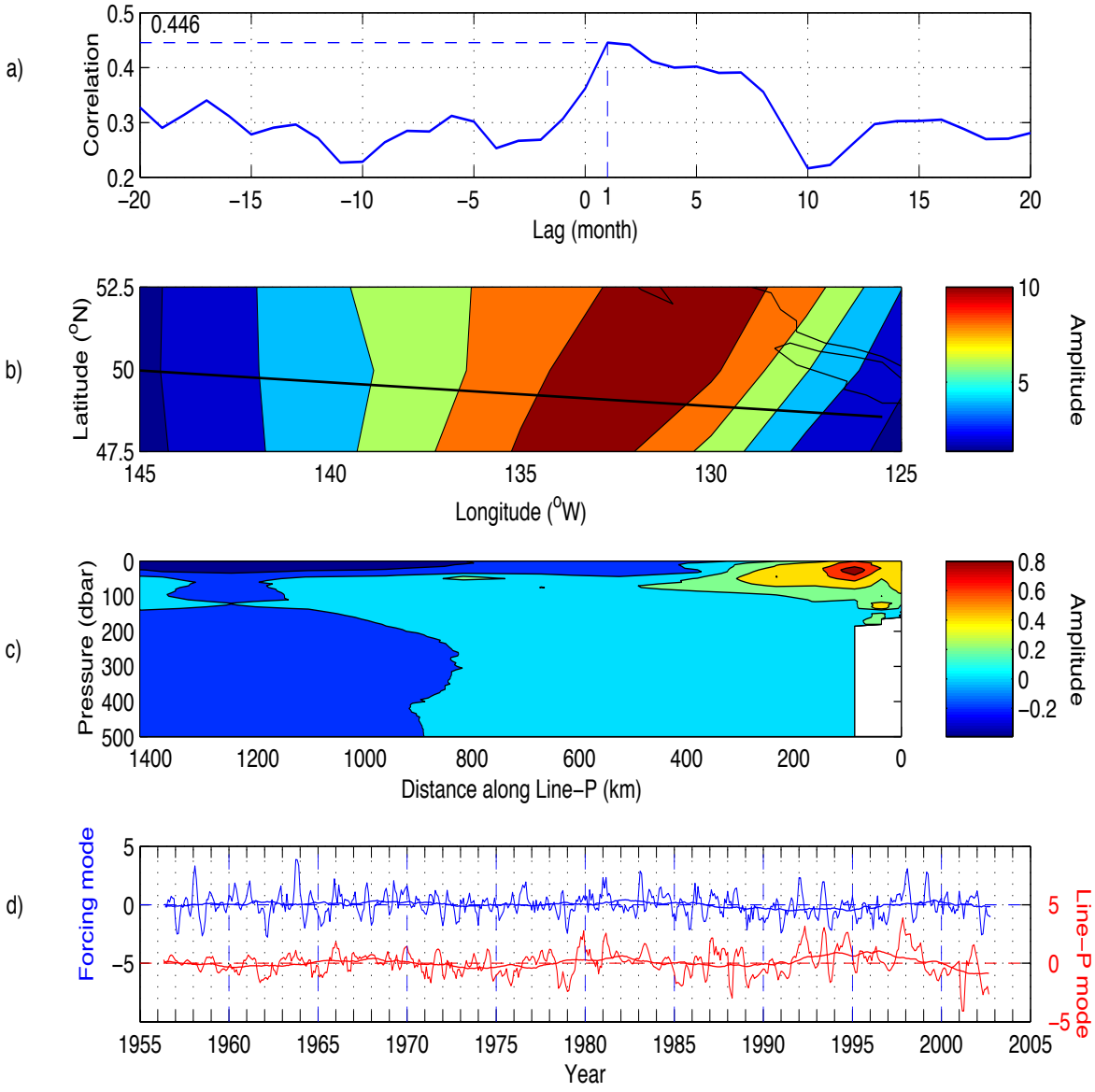

Lag (month)	Variance explained 1	Variance explained 2	Correlation 1	Correlation 2	Significance test
+1	47.2%	12.4%	0.45	0.37	94.0%

Figure 4: CCA between 3 PCs of meridional wind stress anomalies over Line-P and 9 PCs of Line-P temperature anomalies.

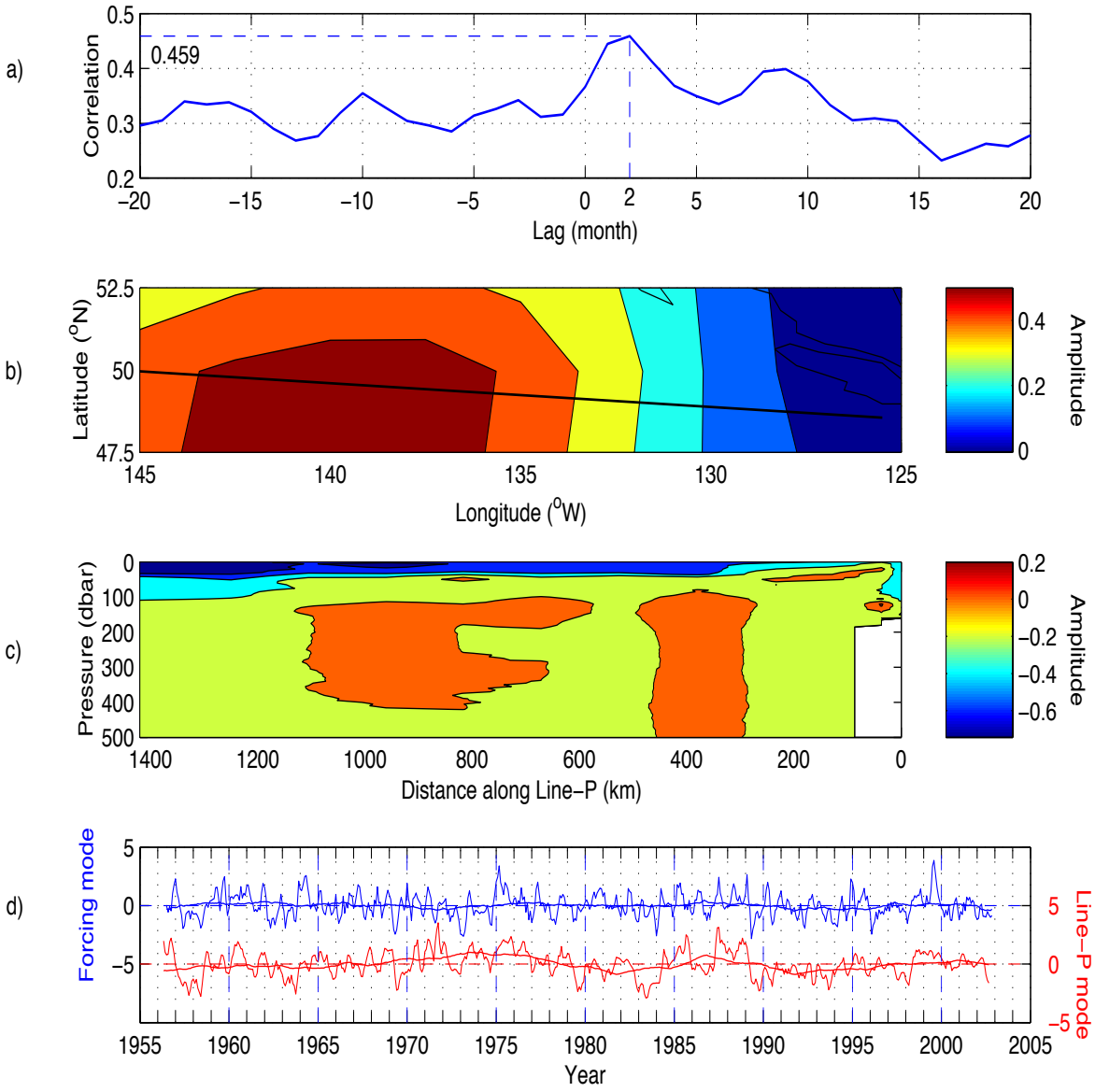

Lag (month)	Variance explained 1	Variance explained 2	Correlation 1	Correlation 2	Significance test
+2	47.6%	12.1%	0.46	0.42	95.1%

Figure 5: CCA between 3 PCs of wind speed anomalies over Line-P and 9 PCs of Line-P temperature anomalies.

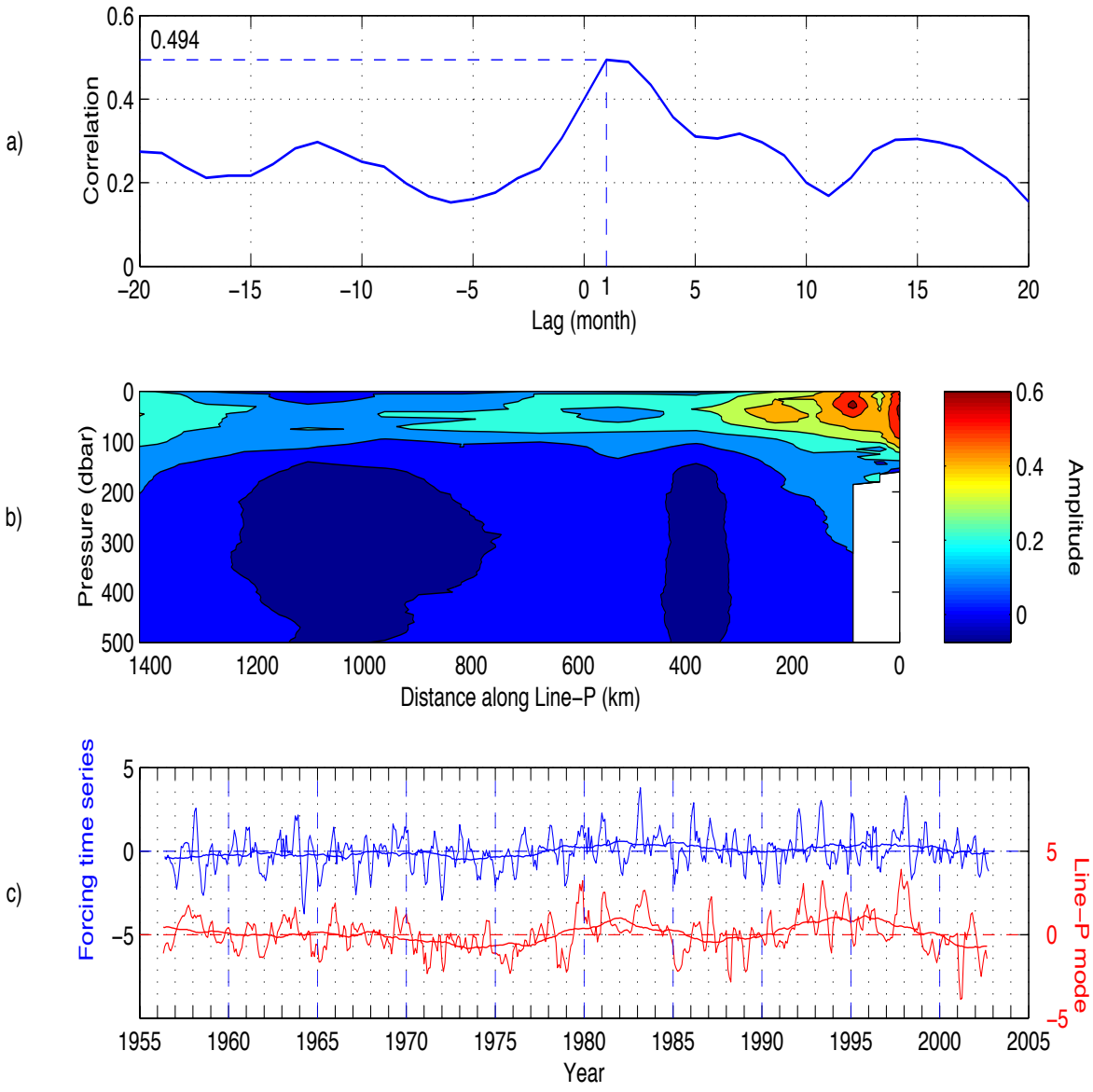

Lag (month)	Variance explained	Correlation 1	Correlation 2	Significance test
+1	12.03 %	0.49	0.49	98.7 %

Figure 6: CCA between wind stress anomalies 15^o counterclockwise from the alongshore direction and 9 PCs of Line-P temperature anomalies. **a)** CCA correlations with lags; **b)** Line-P CCA spatial pattern; **c)** Standardized temporal coefficients for the forcing time series (top) and the Line-P CCA mode (bottom).

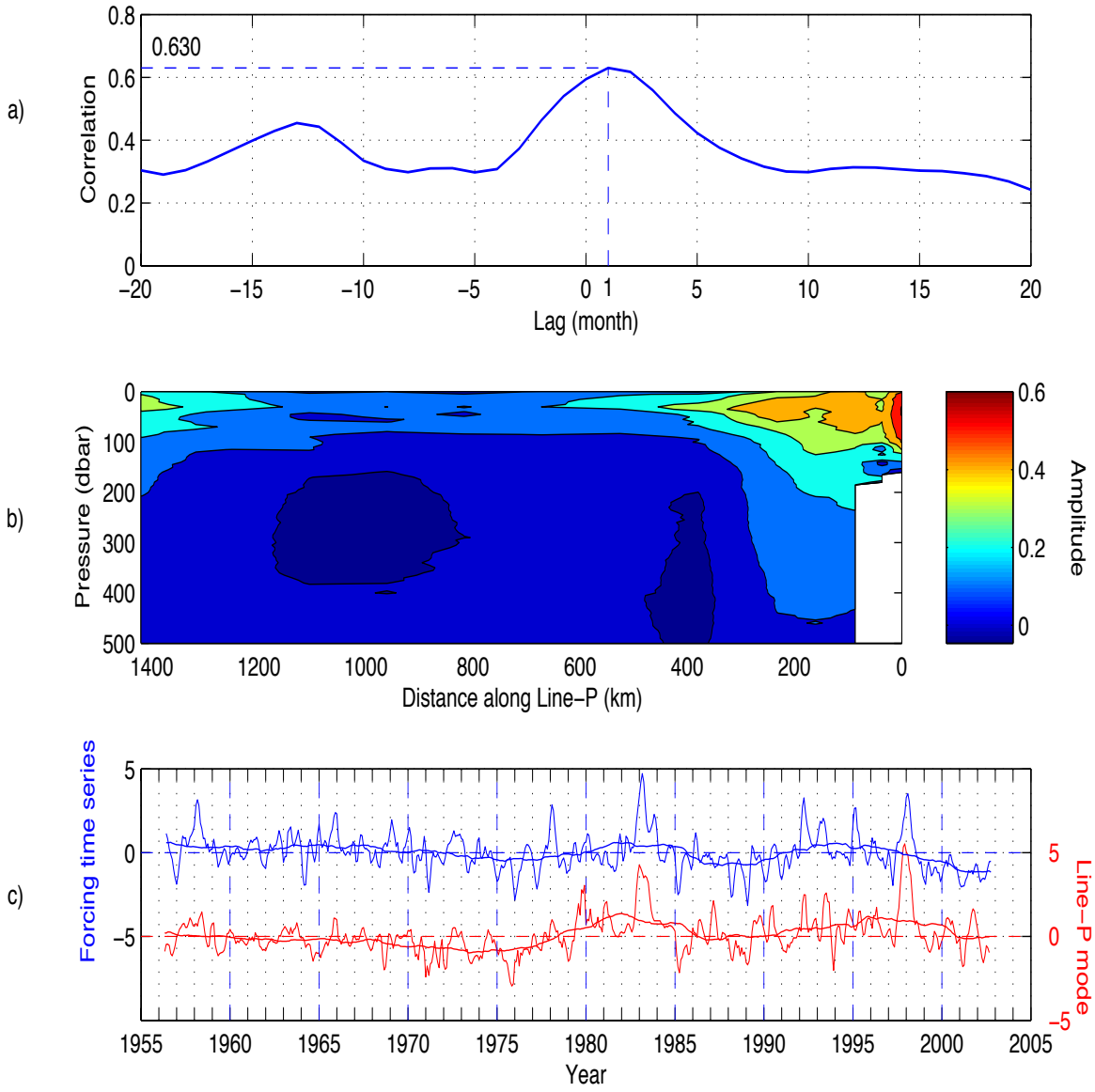

Lag (month)	Variance explained	Correlation 1	Correlation 2	Significance test
+1	12.35 %	0.63	0.56	99.9 %

Figure 7: CCA between SSH anomalies at Crescent City and 9 PCs of Line-P temperature anomalies.